Strain tuning of interorbital correlations in LaVO$_3$ thin films

H. Meley,[1] M. Tran [,][1] J. Teyssier [,][1] J. A. Krieger [,][2,3] T. Prokscha [,][2] A. Suter,[2] Z. Salman [,][2]
M. Viret,[4] D. van der Marel [,][1] and S. Gariglio [1,][*]

[1]*DQMP, University of Geneva, 24 Quai E.-Ansermet, CH-1211 Geneva, Switzerland*
[2]*Laboratory for Muon Spin Spectroscopy, Paul Scherrer Institut, CH-5232 Villigen PSI, Switzerland*
[3]*Laboratorium für Festkörperphysik, ETH Zurich, CH-8093 Zurich, Switzerland*
[4]*SPEC, CEA, CNRS, Université Paris-Saclay, CEA Saclay, F-91191 Gif sur Yvette, France*

$3d^2$ vanadate perovskites exhibit an unusual phase diagram where the low temperature orbital and spin orders are strongly dependent upon the rare-earth cation size. Here, we demonstrate the delicate role of strain in epitaxial LaVO$_3$ films by performing low-energy muon spin spectroscopy and ellipsometry measurements. The electronic structure is revealed by the measurement of the multipeak structure of the charge excitations. The analysis highlights the independent roles of the d_{xy} band confinement and the d_{zx}, d_{zy} doublet polarization for the orbital ordering to establish.

I. INTRODUCTION

In transition metal oxides (TMOs), partially occupied d orbitals experience a strong on-site Coulomb interaction U that leads, for systems with a half-filled conduction band of bandwidth W, to a Mott insulating state [1,2]. The Mott transition has been originally predicted to occur, in the absence of orbital degeneracy, at a critical U/W ratio of ~ 2. It has been shown later that orbitally degenerate materials also undergo a Mott transition with an increased U/W critical ratio [3]. Extending the Mott-Hubbard model to multiband systems in effective Hamiltonians [4–6] has revealed that d electrons in TMOs couple through their orbital and spin degrees of freedom, resulting in orbital/spin-ordered ground states. Nowadays, *ab initio* calculations can correctly predict such states and describe their evolution with temperature (see, for instance, Refs. [7–10]). Advances in thin film synthesis have enabled the study of the complex phase diagrams of these materials and, in particular, the dependence of their electronic properties on the lattice by using epitaxial strain [11,12]. For these compounds, the coupling of the electronic properties to the crystalline structure is indeed important. In the perovskite phase, the fivefold $3d$ orbital degeneracy is lifted by the octahedral coordination of the transition metal (TM) with oxygen, leading to threefold degenerate t_{2g} and twofold degenerate e_g orbital sets. Further crystal-field (CF) splitting can be induced by lattice distortions, such as the orthorhombic ones (GdFeO$_3$ type), which do not affect e_g and t_{2g} orbitals equally. Indeed, the e_g orbital lobes, pointing towards the oxygen atoms (σ bonding), experience a larger Coulomb repulsion than the t_{2g} orbitals, that are pointing away from oxygen (π bonding). Therefore, e_g systems are more prone to a significant Jahn-Teller (JT) coupling that lifts the orbital degeneracy [13] and drives an orbital order (OO), as observed in manganites [10]. The mechanism lifting the t_{2g} orbital degeneracy is more complex since the JT coupling has the same energy scale as the d-d orbital superexchange interaction. These two mechanisms compete in determining the final spin/orbital ground state. The JT coupling, which lifts the t_{2g} state degeneracy via the static structural distortion [14], tends to drive the electronic ground state through a rigid OO upon cooling [15]. On the other hand, the d-d superexchange interaction which lifts the t_{2g} state degeneracy due to the spin/orbital correlation, tends to drive the electronic ground state through a fluctuating-type OO upon cooling [16] [17–21]. In both mechanisms, the ground state spin order (SO) follows the OO symmetry according to the Goodenough-Kanamori-Anderson (GKA) rule [22].

A paradigmatic example of such complexity are the $3d^2$ vanadate perovskites. In their high temperature phase, RVO$_3$ vanadates (R being a rare earth or Y) are paramagnetic Mott insulators with strong three-dimensional (3D) orbital fluctuations where the two d electrons fluctuate between the xy, zx, and zy orbital states. As the temperature is lowered, the system switches from the 3D orbital fluctuation regime to a quasi-1D orbital fluctuation regime [21,23–25]. At the transition temperature T_{OO}, which is in the range 140–200 K depending on the R cation size, the xy orbitals (of lower energy because of the orthorhombic distortion) become singly occupied, while the remaining electron occupies the empty zx or zy orbitals. Two different ground states are observed depending on the zx, zy orbital arrangement along the z axis as shown in Fig. 1 [26]: The orbital singlet that consists of an antiferro orbital arrangement along z (G-type OO and C-type SO) and the orbital triplet that consists of a ferro orbital arrangement along z (C-type OO and G-type SO).

The observed OO in LaVO$_3$ is a condensation of the orbital singlet state (G-type OO and C-type SO), although the JT coupling lifts the zx, zy degeneracy [27], i.e., polarizes the $\{zx/zy\}$ doublets. This fact reflects the rather weak JT coupling that is not strong enough to balance the superexchange-mediated d-d
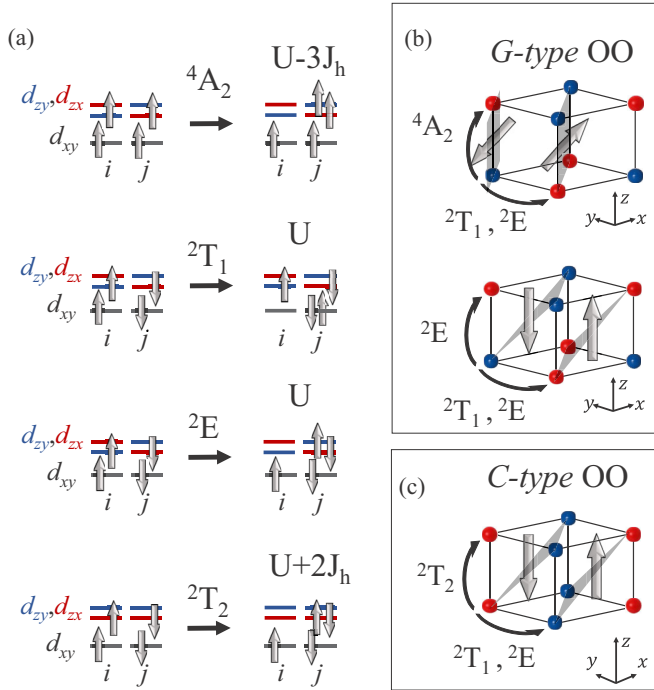
*stefano.gariglio@unige.ch

FIG. 1. (a) The multiplet representation of the four first charge excitations for a cubic $3d^2$ transition metal oxide with t_{2g} orbitals [23]. The xy (black), zy (blue), zx orbitals (red), and spin (gray arrows) are represented. The transition to the high-spin state ($^4A_2$) has the lowest excitation energy $U - 3J_h$. The low-spin transition with electrons in different orbitals ^2E has an excitation energy U. The low-spin transitions with the electrons on the same orbitals ($^2T_1$ and $^2T_2$) have excitations energies of U and $U + 2J_h$, respectively. (b) Illustration of the two allowed antiferromagnetic (AFM) SO assuming the G-type OO: The ground state observed for LaVO$_3$ is the C-type SO (ferromagnetic chains along z with the lower energy excitation energy $U - 3J_h$). (c) Assuming the C-type OO, only the G-type SO is allowed. (b) and (c) The excitations involved per spin/orbital bond are marked by the black arrows. In the 1D orbital fluctuation regime, the spin/orbital bonds fluctuate between the three possible arrangements; as the temperature decreases, the G-type OO/C-type SO ground state sets in for LaVO$_3$.

interaction. This interplay between the lattice-orbital coupling and the electronic correlations has been extensively debated to explain the complex phase diagram of the $3d^2$ vanadates, whose ground state turns out to be highly susceptible to small changes in the internal distortions [21,28–30]. Our purpose with the present work is to alter the LaVO$_3$ $zy/zx/xy$ energy levels and bandwidths using the epitaxial strain. We highlight the independent roles of the xy band confinement and of the $\{zx, zy\}$ doublet polarization for the establishment of the OO and SO. We show that by changing the sign of the applied biaxial strain we can alter the LaVO$_3$ OO transition either by enhancing the 1D quantum orbital fluctuation regime or by maintaining the bulk one.

In detail, we grow LaVO$_3$ films on top of two different substrates to tune the octahedral rotations, and consequently, the crystal-field (CF) splitting. Using muon spin relaxation (μSR) and ellipsometry, we detect the onset of the antiferromagnetic spin ordering temperature and probe the film optical conduc-

tivity as a function of temperature. The epitaxial strain alters the multipeak structure of the optical conductivity as well as the spin/orbital ordering transition temperatures [31,32]. For the compressive system (LaVO$_3$ on SrTiO$_3$), the temperature dependence of the optical excitations is very similar to the bulk one [25] with a spin ordering lowered to $T_{SO} = 125$ K and an orbital ordering occurring at $T_{OO} = 135$ K, while in bulk both occur around 140 K. The OO (3D to 1D regime transition) manifests in an abrupt change in the optical spectra at T_{OO}, as in the bulk. For the tensile system (LaVO$_3$ on DyScO$_3$), the spin ordering transition is increased to 155 K while the optical spectra, drastically different from previous LaVO$_3$ bulk measurements [25], evolve smoothly in temperature, a behavior that reflects the progressive establishment of the 1D fluctuating-type OO upon cooling.

II. EXPERIMENTAL DETAILS

LaVO$_3$ thin films were grown by pulsed laser deposition using a ceramic target of LaVO$_4$ in an oxygen pressure of 10^{-7} mbar at $900\,^\circ$C (for details, see Ref. [33]). Their thickness was 80 nm. The use of two different substrates [(001) SrTiO$_3$ and (110)$_o$DyScO$_3$] allows us to apply a strain of $\sim -0.5\%$ and $\sim +0.5\%$, respectively. In a previous study we have observed that the strain state determines the orientation of the orthorhombic cell on the substrate. The compressive strain provided by SrTiO$_3$ induces an in-plane orientation of the long orthorhombic (c_o) axis. On the contrary, the tensile strain induced by DyScO$_3$ leads to an out-of-plane c_o axis orientation [33]. In the following, we use the film orthorhombic unit cell as a reference for the directions of a_o, b_o, and c_o, choosing, for the orbitals, the xy plane to be perpendicular to c_o.

One way to probe the spin-orbital correlations and their evolution in temperature is to perform optical spectroscopy [34] combined with μSR. In the μSR measurement, spin-polarized muons are used as a probe to detect the distribution of the local magnetic field inside the sample: It is a highly sensitive technique for magnetic transitions that is used here to reveal the onset of the antiferromagnetic order. The μSR measurements were performed in a small transverse magnetic field of 5 mT (TF-μSR measurements) at the μE4 beamline of the Paul Scherrer Institute in Switzerland [35,36] and analyzed by MUSRFIT [37]. The results shown here were obtained by using an implantation energy of 7 keV, which corresponds to the muons stopping approximately in the middle of the LaVO$_3$ film. However, additional measurements as a function of implantation energy in the range of 4–18 keV revealed no variation of the magnetic state across the film. We also performed a few measurements in zero field (ZF-μSR measurements) to detect the spontaneous precession signal in the local field, a technique that gives evidence of the presence of a long range magnetic order in the samples [38].

III. RESULTS AND DISCUSSIONS

TF-μSR asymmetry spectra, measured in both films at various temperatures, are shown in Fig. 2. The data exhibit a damped oscillating behavior, which can be fitted to

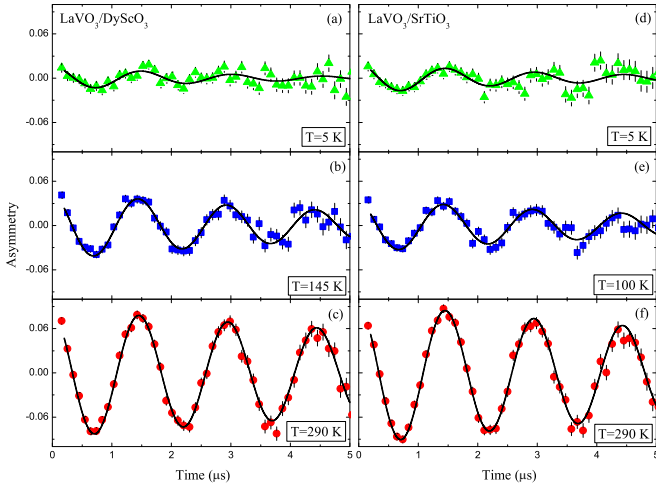$$A(t) = A_0\, e^{-\lambda t} \cos(\omega t + \varphi),$$

FIG. 2. Typical asymmetry spectra measured at various temperatures using an implantation energy of 7 keV: In (a)–(c) are shown the data of $LaVO_3/DyScO_3$ and in (d)–(f) the ones of $LaVO_3/SrTiO_3$ films. The lines indicate the best fit using the formula presented in the text.

where A_0 is the initial amplitude of the asymmetry, λ is the damping rate of the oscillation amplitude, ω the (Larmor) precession frequency, t the time, and φ is the initial phase of the precession which depends on the initial direction of the muon spin and the geometry of the positron detectors. The precession frequency ω is proportional to the mean local field (B_l) experienced by the muons, $\omega = \gamma_\mu B_l$, where $\gamma_\mu = 2\pi \times 135.5$ MHz/T is the muon gyromagnetic ratio. The damping rate λ is a measure of the width of the local field distribution. The temperature evolution of the initial muon spin polarization inferred from A_0 is plotted in Fig. 4 for the two strain states. Note that due to broad internal magnetic field distributions, a magnetic state in a transverse field can cause an effective loss of initial muon spin polarization [39]. At a critical temperature we observe a sharp drop in the spin polarization, that is due to the appearance of strong static magnetic fields in the sample: We define this temperature as the spin ordering temperature and estimate $T_N = 125$ K for $LaVO_3$ on $SrTiO_3$ and 155 K on $DyScO_3$.

To probe the electronic evolution of these insulating layers we resorted to optical spectroscopy. In an ellipsometry measurement, the change in temperature of the optical spectra along the different crystallographic axes of the films reveals the evolution of the kinetic terms involved per spin-orbital bond [23]. In a correlated insulator, the different d-d optical excitation energies are ruled by the local interactions. Since it is now accepted that the occupancy of the xy orbital becomes one below T_{OO} [21,27,40], the different virtual low-energy d-d excitations $d_i^2 d_j^2 \rightarrow d_i^1 d_j^3$ involve only the zx, zy orbital doublets and the half-filled xy orbitals. Taking into account the intraorbital interaction U and the Hund's exchange interaction J_h [23], different Mott-Hubbard (MH) excitations are expected as shown in Fig. 1: the high-spin $^4A_2$ transition of energy $U - 3J_h$ and the three low-spin transitions $^2T_1$, ^2E, and $^2T_2$ of energies U, U, and $U + 2J_h$ (the last one is above our experimental energy range). With an energy between U and $U + 2J_h$, there is also a charge-transfer (CT) p-d transition.
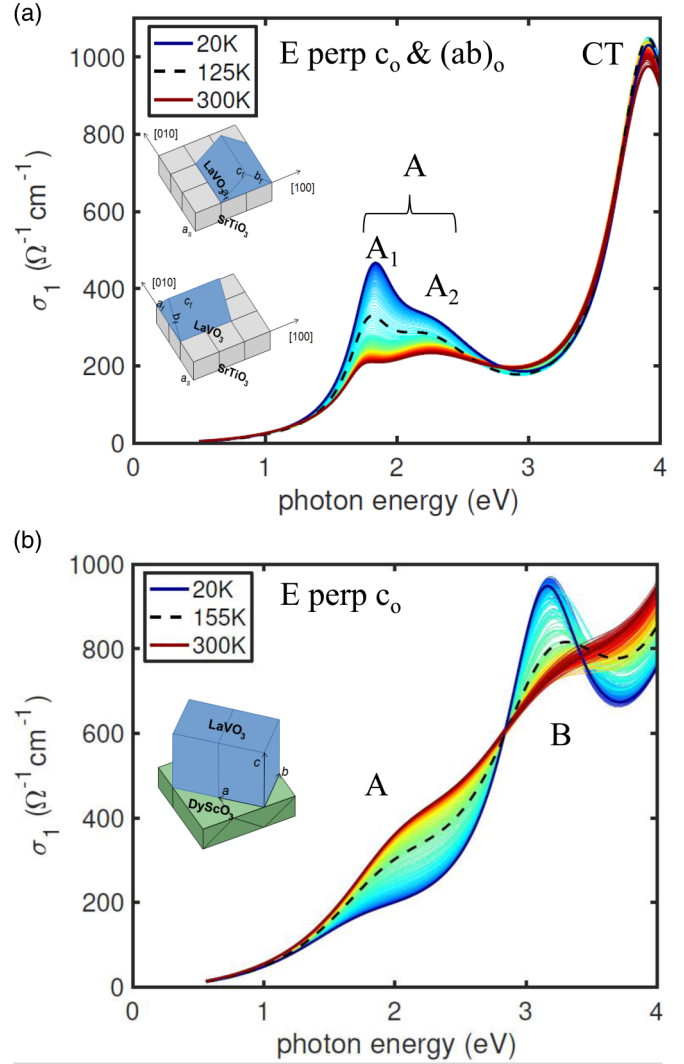

FIG. 3. Plot of the temperature dependent optical conductivity vs energy for (a) a $LaVO_3$ layer on top of $SrTiO_3$, where the incident beam is polarized perpendicularly to both c_o and $(ab)_o$ axes, and (b) a $LaVO_3$ layer on top of $DyScO_3$, where E is perpendicular to c_o axis. In both plots, the temperature of the antiferromagnetic order T_{SO} is marked by the dashed black line.

The ellipsometry measurement has been performed using a rotating analyzer and the optical analysis uses a Kramers-Kronig strain variational method, implemented in a software by Kuzmenko [41], modeling the system as an orthorhombic film on a substrate. Taking the reported bulk values of $U \sim 3$–3.6 eV for the on-site Coulomb interaction (intraorbital), and of $J_h \sim 0.4$–0.7 eV for the Hund's exchange interaction, with a CT excitation peak of around 4.5 eV [24,29,42–44], we can identify in our optical spectra shown in Fig. 3 the double peak A (1.8–2.2 eV) as the $^4A_2$ multiplet and the peak B (3.1 eV) as the $^2T_1$, ^2E multiplets.

Considering a G-type OO and a C-type SO ferromagnetic (FM) spin arrangement along the c_o axis and antiferromagnetic (AFM) along the ab_o direction, as sketched in Fig. 1(b), an increase of the spectral weight (SW) of peak A upon cooling is expected only along the c_o axis [45]. This strong anisotropy has been observed on RVO_3 single crystals
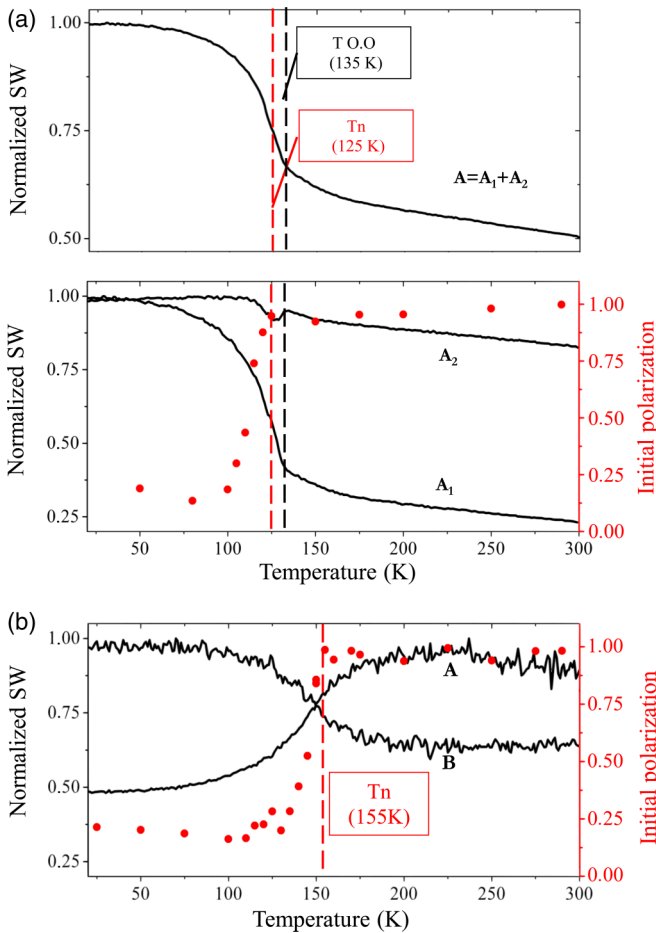
FIG. 4. (a) Black curve: SW of peak A_1, A_2 and their sum (A) for the compressive LaVO$_3$ layer. In red: The muon initial spin polarization revealing the occurrence of the antiferromagnetic order (T_N) at 125 K. (b) Black curve: SW of peak A and peak B for the LaVO$_3$ layer under tensile strain. In red: The muon initial spin polarization drops when the antiferromagnetic order sets in at 155 K.

(R = La, Ce, Cd, and Y) with a transition temperature ranging from 140 to 200 K [24,25]. On the other hand, considering a C-type OO, an increase of the SW of peak B is expected along both the c_o and the ab_o axes [23,45]. This effect has been observed in the low temperature phase of YVO$_3$ [24]. Along the ab direction, one would expect the evolution of the SW to be independent of the two types of OO. Indeed, whether it is a C or G type, only the low-spin transitions of energy U are allowed by the in-plane AFM spin arrangement [see Fig. 1(b)], i.e., a transfer of spectral weight from the low-energy peak (A) to the high-energy one (B) is expected upon cooling [45].

The optical spectra measured on the LaVO$_3$ thin films are shown in Fig. 3. For the film under compressive strain [Fig. 3(a)], the spectra are similar to the ones of bulk LaVO$_3$: The peak A (high-spin excitation) splits in two peaks A_1 (1.8 eV) and A_2 (2.3 eV), where the first is attributed to an exciton and the second to a MH transition [46]. As in bulk LaVO$_3$, the signature of the G-type OO manifests in a gain of SW of peak A below T_{OO}. Note that in bulk, it is mainly σ_c that is evolving. In the present case (compressive strain),

the measured optical conductivity σ_1 is a mixture of σ_c and σ_{ab} due to the presence of 90° c_o domains [47]. The film under tensile strain [Fig. 3(b)] is oriented with the c_o axis out of plane, so that only σ_{ab} is measured. Here, in contrast to the bulk LaVO$_3$, both peaks A and B are present. Going across the OO transition, one notices a transfer of SW from peak A to peak B. We note that although this SW transfer along σ_{ab} is expected for both the G- and C-type OO [45], the only transition in bulk that clearly shows this behavior is the low temperature C-type OO observed on YVO$_3$ [24]. Optical conductivity for compounds characterized by a G-type OO such as LaVO$_3$ shows almost no change of SW in the ab_o plane [24,25,48] and no peak B.

From these measurements, we extract the SW of the different peaks using the optical conductivity sum rule [41]. The result is shown in Fig. 4. For the LaVO$_3$ layer under compressive strain (c_o axis in plane), the temperature dependence of the SW of peak A shows a clear kink at T_{OO} (135 K) [see Fig. 4(a)]. Looking at the evolution of its two components (A_1 and A_2), one notices a second discontinuity affecting the SW of peak A_2 at 125 K: This temperature coincides with the spin ordering temperature, as evidenced by the drop at 125 K in the muon initial polarization, so that we relate this second change in spectral weight to the spin transition. This observation confirms that the kink at 135 K indicates the orbital ordering temperature. The evolution in temperature of the SW of peak A reproduces the behavior observed on RVO$_3$ single crystals going across the orbital transition towards a G-type order [24,25]. We claim that the presence of kinks at the OO temperature is the signature of the localization of the xy orbital state, concomitant with the establishment of the 1D zy, zx doublet fluctuation regime [20,23]. For the LaVO$_3$ layer under tensile strain, the SW transfer from peak A to peak B shows no kink at the spin ordering temperature: T_{SO} is again revealed by the drop in the muon initial polarization at 155 K. The smooth evolution of the SWs in the range of the measured temperature [see Fig. 4(b)] indicates the free establishment of the 1D orbital fluctuation regime upon cooling, i.e., that the 1D regime is not quenched by the 3D orbital fluctuations.

The effect of strain on the CF splittings and hopping amplitudes (bandwidths) of the bulk LaVO$_3$ has already been investigated by density functional theory (DFT) [31,32]. When biaxial strain is applied on a 100_{pc} oriented unit cell, the in- and out-of-plane octahedral rotations are affected as well as the CF splitting. For a compressive/tensile strain, the calculations predict an increase/decrease of the octahedral rotations about the out-of-plane direction and a decrease/increase of the octahedral rotations about the axes in the epitaxial plane. These changes are concomitant with an extra tetragonal CF splitting. In our case, the strain level ($\pm 0.5\%$) is expected to generate an extra split of ~ 0.06 eV [31] between the in-plane orbital (epitaxial plane) and the two others. Also, the downward/upward shifting of the orbital energy levels is respectively accompanied by a decrease/increase of the first neighbor hopping amplitudes ($\sim \pm 0.25$ eV). As a result, orbital states whose energy levels are shifted down see their bandwidth decrease and tend to localize and vice versa (see Fig. 5). We therefore expect the layer under tensile strain with c_o perpendicular to the interface
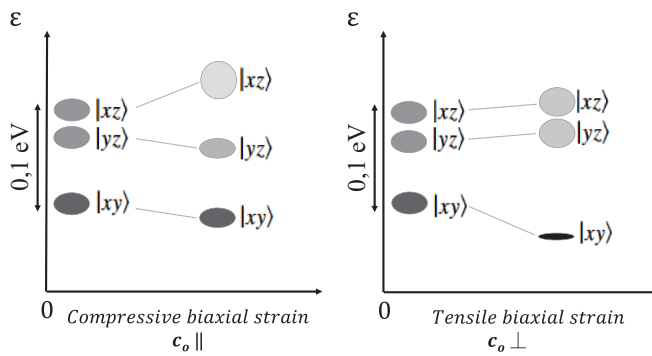
FIG. 5. Schematic representation of the epitaxial strain effect on the CF splitting and bandwidth of the V t_{2g} orbitals. In the zero-strain state, the xy, yz, and xz orbitals are split by an absolute value of ~ 0.1 eV [32]. Left side: A compressive epitaxial strain is applied to the zx plane, which increases the original CF splitting between xz and yz orbitals. Right side: A tensile epitaxial strain is applied to the xy plane, increasing the original CF splitting between the xy and the yz/xz orbital states. The strain-induced energy levels shifting ($\sim \pm 0.06$ eV) are accompanied by a decrease or increase of the first neighbor hopping amplitudes ($\sim \pm 0.25$ eV), which manifests in a bandwidth decrease or increase [32].

to stabilize the zx, zy doublet via the xy orbital confinement and therefore enhance the material propensity to reach the 1D orbital fluctuation regime. T_{SO} is indeed increased by 15 K and the smooth onset of the OO starts 50 K above the bulk OO temperature (see Fig. 4). On the other hand, the compressive strain with c_o parallel to the interface induces a polarization of the zx, zy doublet (see Fig. 5), that adds on top of the bulk natural CF splitting and goes against the G-type OO. Indeed, the SO and OO transition temperatures are lowered by 15 and 10 K, respectively (see Fig. 4).

IV. SUMMARY

Unveiling the electronic structure of the layers by identifying the charge excitations, we have demonstrated the sensitive role of strain in epitaxial LaVO$_3$ films. Following the SW evolution of the different peaks as a function of temperature, we shed light on the OO origin. Altering the CF using biaxial strain allowed us to identify the roles of the xy band confinement and of the $\{zx, zy\}$ doublet correlations for the OO and SO establishment: (1) The use of compressive strain on LaVO$_3$, that increases the zx, zy doublet polarization, did not suppress the bulk G-type orbital order driven by the d-d correlations, and only a substantial decrease of the bulk spin and orbital order transition temperature is observed, confirming the rather weak orbital-lattice JT coupling. Moreover, despite the locking of the c_o axis by the substrate and the absence of a structural transition (no reduction of the unit cell volume measured by temperature-dependent x-ray diffraction [33]), the optical signature at the OO/SO remains quasi-identical to the bulk one. These observations unambiguously show that the bulk structural transition indeed originates from the d-d orbital correlations. (2) The use of tensile strain that lowers the xy energy levels is believed to increase the 3D to 1D transition temperature, thereby allowing the zx, zy doublet fluctuations to persist to higher temperatures than in the bulk. This expected enhancement of the 1D quantum orbital fluctuations at high temperatures is indeed confirmed by the observation of the smooth evolution of the SW in temperature, up to 180 K.

[1] N. Mott and R. Peierls, Proc. Phys. Soc. **49**, 72 (1937).

[2] N. Mott, Proc. Phys. Soc. A **62**, 416 (1949).

[3] O. Gunnarsson, E. Koch, and R. M. Martin, Phys. Rev. B **56**, 1146 (1997).

[4] K. Kugel and D. Khomskii, JETP Lett. **15**, 446 (1972).

[5] M. Cyrot and C. Lyon-Caen, J. Phys. France **36**, 253 (1975).

[6] S. Inagaki, J. Phys. Soc. Jpn. **39**, 596 (1975).

[7] H. Park, A. J. Millis, and C. A. Marianetti, Phys. Rev. Lett. **109**, 156402 (2012).

[8] A. Mercy, J. Bieder, J. Íñiguez, and P. Ghosez, Nat. Commun. **8**, 1677 (2017).

[9] S. Johnston, A. Mukherjee, I. Elfimov, M. Berciu, and G. A. Sawatzky, Phys. Rev. Lett. **112**, 106404 (2014).

[10] Y. Tokura, Rep. Prog. Phys. **69**, 797 (2006).

[11] D. Schlom, L.-Q. Chen, X. Pan, A. Schmehl, and M. A. Zurbuchen, J. Am. Ceram. Soc. **91**, 2429 (2008).

[12] S. Catalano, M. Gibert, V. Bisogni, O. Peil, F. He, R. Sutarto, M. Viret, P. Zubko, R. Scherwitzl, A. Georges, G. Sawatzky, T. Schmitt, and J.-M. Triscone, APL Mater. **2**, 116110 (2014).

[13] A. J. Millis, B. I. Shraiman, and R. Mueller, Phys. Rev. Lett. **77**, 175 (1996).

[14] M. Imada, A. Fujimori, and Y. Tokura, Rev. Mod. Phys. **70**, 1039 (1998).

[15] Rigid orbital ordering describes an orbital order transition that is driven by the lattice distortions .

[16] Fluctuating-type OO is ruled by strong quantum fluctuations of the orbital dynamics, that are slowly reduced as the OO sets in. These fluctuations between different quantum states originate from the orbital degeneracy and from the structure of the spin/orbital superexchange that allows both ferromagnetic and antiferromagnetic spin/orbital arrangements along each bond .

[17] K. Kugel' and D. Khomskiĭ, Sov. Phys. Usp. **25**, 231 (1982).

[18] G. Khaliullin, P. Horsch, and A. M. Oleś, Phys. Rev. Lett. **86**, 3879 (2001).

[19] D. Khomski and M. Mostovoy, J. Phys. A: Math. Gen. **36**, 9197 (2003).

[20] G. Khaliullin, P. Horsch, and A. M. Oles, Phys. Rev. B **70**, 195103 (2004).

[21] G. Khaliullin, Prog. Theor. Phys. Suppl. **160**, 155 (2005).

[22] J. Kanamori, J. Phys. Chem. Solids **10**, 87 (1959).

[23] A. M. Oleś, G. Khaliullin, P. Horsch, and L. F. Feiner, Phys. Rev. B **72**, 214431 (2005).

[24] J. Reul, A. A. Nugroho, T. T. M. Palstra, and M. Grüninger, Phys. Rev. B **86**, 125128 (2012).

[25] S. Miyasaka, Y. Okimoto, and Y. Tokura, J. Phys. Soc. Jpn. **71**, 2086 (2002).

[26] The in-plane antiferro orbital arrangement is triggered by the classical xy OO that imposes an antiferromagnetic SO(AFM superexchange) [21] while the in-plane antiferro orbital arrangement is supported by the cooperative JT coupling.

[27] G. R. Blake, T. T. M. Palstra, Y. Ren, A. A. Nugroho, and A. A. Menovsky, Phys. Rev. Lett. **87**, 245501 (2001).

[28] M. De Raychaudhury, E. Pavarini, and O. K. Andersen, Phys. Rev. Lett. **99**, 126402 (2007).

[29] C. Ulrich, G. Khaliullin, J. Sirker, M. Reehuis, M. Ohl, S. Miyasaka, Y. Tokura, and B. Keimer, Phys. Rev. Lett. **91**, 257202 (2003).

[30] I. V. Solovyev, Phys. Rev. B **74**, 054412 (2006).

[31] G. Sclauzero and C. Ederer, Phys. Rev. B **92**, 235112 (2015).

[32] G. Sclauzero, K. Dymkowski, and C. Ederer, Phys. Rev. B **94**, 245109 (2016).

[33] H. Meley, Karandeep, L. Oberson, J. de Bruijckere, D. Alexander, J.-M. Triscone, P. Ghosez, and S. Gariglio, APL Mater. **6**, 046102 (2018).

[34] A. Chattopadhyay, A. J. Millis, and S. Das Sarma, Phys. Rev. B **61**, 10738 (2000).

[35] E. Morenzoni, H. Glückler, T. Prokscha, H. Weber, E. Forgan, T. Jackson, H. Luetkens, C. Niedermayer, M. Pleines, M. Birke, A. Hofer, J. Litterst, T. Riseman, and G. Schatz, Physica B **289-290**, 653 (2000).

[36] T. Prokscha, E. Morenzoni, K. Deiters, F. Foroughi, D. George, R. Kobler, A. Suter, and V. Vrankovic, Nucl. Instrum. Methods Phys. Res. **595**, 317 (2008).

[37] A. Suter and B. Wojek, Phys. Proc. **30**, 69 (2012).

[38] See Supplemental Material at http://link.aps.org/supplemental/10.1103/PhysRevB.103.125112 for details on measurement techniques and data analysis, and additional μSR spectra.

[39] A. Yaouanc and P. de Réotier, *Muon Spin Rotation, Relaxation, and Resonance: Applications to Condensed Matter* (Oxford University Press, Oxford, U.K., 2011).

[40] P. Bordet, C. Chaillout, M. Marezio, Q. Huang, A. Santoro, S.-W. Cheong, H. Takagi, C. Oglesby, and B. Batlogg, J. Solid State Chem. **106**, 253 (1993).

[41] A. B. Kuzmenko, Rev. Sci. Instrum. **76**, 083108 (2005).

[42] T. Arima, Y. Tokura, and J. B. Torrance, Phys. Rev. B **48**, 17006 (1993).

[43] A. A. Tsvetkov, F. P. Mena, P. H. M. van Loosdrecht, D. van der Marel, Y. Ren, A. A. Nugroho, A. A. Menovsky, I. S. Elfimov, and G. A. Sawatzky, Phys. Rev. B **69**, 075110 (2004).

[44] E. Benckiser, R. Rückamp, T. Möller, T. Taetz, A. Möller, A. A. Nugroho, T. T. M. Palstra, G. S. Uhrig, and M. Grüninger, New J. Phys. **10**, 053027 (2008).

[45] M. Kim, Phys. Rev. B **97**, 155141 (2018).

[46] F. Novelli, D. Fausti, J. Reul, F. Cilento, P. H. M. van Loosdrecht, A. A. Nugroho, T. T. M. Palstra, M. Grüninger, and F. Parmigiani, Phys. Rev. B **86**, 165135 (2012).

[47] Domains have their c_o axis oriented along the two in-plane crystallographic directions of the substrate .

[48] Y. Motome, H. Seo, Z. Fang, and N. Nagaosa, Phys. Rev. Lett. **90**, 146602 (2003).